Chinese Chemical Letters 31 (2020) 2235–2238

Contents lists available at ScienceDirect

Chinese Chemical Letters

journal homepage: www.elsevier.com/locate/cclet

Communication

One-step synthesis of biomass derived O, N-codoped hierarchical porous carbon with high surface area for supercapacitors

Shuxian Sun[a], Fuqin Han[a], Xiaoliang Wu[a,*], Zhuangjun Fan[b,*]

[a] College of Chemistry, Chemical Engineering and Resource Utilization, Northeast Forestry University, Harbin 150040, China
[b] College of Material Science and Engineering, China University of Petroleum, Qingdao 266580, China

ARTICLE INFO

Article history:
Received 25 September 2019
Received in revised form 12 November 2019
Accepted 13 November 2019
Available online 15 November 2019

Keywords:
Alginic acid
Urea
$KHCO_3$
Supercapacitors
Hierarchical porous carbon

ABSTRACT

We report a convenient method to synthesize O, N-codoped hierarchical porous carbon by one-step carbonization of the mixture of $KHCO_3$, urea and alginic acid. Benefiting from $KHCO_3$ and urea synergistic effect, the obtained O, N-codoped hierarchical porous carbon (NPC-700) material has a well-developed interconnected porous framework with ultrahigh specific surface area (2846 m^2/g) and massive heteroatoms functional groups. Consequence, such porous carbon displays high specific capacitance (324 F/g at 1 A/g), excellent rate performance (212 F/g at 30 A/g) and good electrochemical stabilization in 6 mol/L KOH solution. More importantly, the assembled NPC-700//NPC-700 symmetrical supercapacitor can achieve a high energy density of 18.8 Wh/kg and good electrochemical stabilization in 1 mol/L Na_2SO_4 solution. This process opens up a new way to design heteroatoms-doped hierarchical porous carbon derived from biomass materials for supercapacitors.

Supercapacitors have got extensive concerns in recent decades because of the advantages of ultrahigh power density, fast charge and discharge response, long cycling life and environmental-friendly [1,2]. Carbon materials, especially activated carbons (ACs) play an important role in double-layer capacitors (EDLCs) owing to the high specific surface area, low cost and excellent electrochemical stabilization [3–5]. ACs usually can be obtained by carbonization of carbon precursors and followed by activation in inert gas. However, such porous carbons are faced with poor conductivity, large ion-transport resistance and long ion-diffusion distance caused by their amorphous microporous structure, resulting in unsatisfactory supercapacitive performance [6,7].

Three-dimensional (3D) interconnected hierarchical porous carbon with high specific surface area displays excellent electrochemical performance has drawn numerous attentions in recent years [6,8]. Micropores (< 2 nm) can provide a larger specific surface area to absorb electrolyte ions, mesopores (2−50 nm) can be used as rapid channels for diffusion of ions, and macropores (> 50 nm) can be used as ion buffer pools to shorten the diffusion distance of ions. Thus, 3D interconnected hierarchical porous carbon can not only offer high specific surface area to store energy, but also shorten ion diffuse route, which can greatly enhance the supercapacitive performance [9]. Template method is the main method to prepare 3D hierarchical porous carbon, which contains complex preparation process with template preparation, removal, and post-activation [10,11]. Apart from adjusting pore structure, another effective method to enhance the electrochemical property of carbon materials is doping heteroatoms (*e.g.*, N, O and S atoms) in carbon framework [12–15]. Especially, N/O heteroatom doping is considered as a promising method for enhancing the electrochemical performance of carbon materials. The oxygen and nitrogen functional groups can not only improve wettability, but also offer extra pseudocapacitance during charging and discharging process [16–18]. Therefore, developing a convenient method to prepare 3D interconnected hierarchical porous carbon with suitable heteroatom functional groups is highly desirable for high-performance supercapacitor.

Herein, we develop a simple strategy to prepare nitrogen and oxygen codoped hierarchical porous carbon through one-step pyrolysis of the mixture of $KHCO_3$, urea and alginic acid. Benefiting from $KHCO_3$ and urea synergistic effect, the obtained O, N-codoped hierarchical porous materials possess a well-developed hierarchical porous framework with ultrahigh specific surface area and rich heteroatoms functional groups. As a result, such porous carbon displays high specific capacitance and good electrochemical stabilization in 6 mol/L KOH solution. More importantly, the constructed NPC-700//NPC-700 symmetrical supercapacitor shows high energy density and good cycling stability in 1 mol/L Na_2SO_4 solution.

* Corresponding authors.
E-mail addresses: wuxiaoliang90@163.com (X. Wu), fanzhj666@163.com (Z. Fan).

https://doi.org/10.1016/j.cclet.2019.11.023

The micromorphology of the prepared materials was tested through scanning electron microscopy (SEM) and transmission electron microscopy (TEM). As presented in Fig. S1a (Supporting information), the CC-700 materials show an irregular block structure without obvious pore structure. The PC-700 exhibits 3D interconnected porous structure, indicating that the $KHCO_3$ can significantly affect the formation of the interconnected porous structure. As presented in Figs. 1a and b, similar with PC-700, the NPC-700 samples exhibit 3D highly interconnected porous framework with sub-micrometer sized macropores. This unique structure can greatly shorten the ion transport distance to the interior surfaces and enhance the availability of active materials. Moreover, the corresponding element mapping images (Fig. 1d) exhibit the uniform distribution of C (Fig. 1e), O (Fig. 1f) and N (Fig. 1g) atoms. The TEM image of NPC-700 (Fig. 1c) further confirms 3D interconnected porous framework with the sizes of macropores ranging from 1 μm to 2 μm. The high-resolution TEM image of NPC-700 displays rich micropores in the carbon framework (Fig. S2 in Supporting information), which is in favor of energy storage.

From X-ray power diffraction patterns (Fig. 2a), all materials show two wide characteristic peaks at about $2\theta = 23°$ and $2\theta = 43.6°$, corresponding to the (002) and (100) crystal planes of carbon materials, which reveal the disorder nature and partial graphitized character [19]. The (002) peak of NPC-700 sample is broader and weaker compared with CC-700 and PC-700, indicating the increase of disordered structure and presence of high-density micropores. Raman spectra further investigate the disordered structure of NPC-700. Two feature peaks at 1340 and 1580 cm^{-1} are observed, corresponding to D band (disordered carbon) and G band (graphite phase), respectively (Fig. 2b) [20]. The I_D/I_G ratio of NPC-700 is 0.95, indicating the existence of disordered structure. The surface element of NPC-700 was measured by X-ray photoelectron spectroscopy. As presented in Fig. 2c, the NPC-700 sample possesses high content of O (14.75 at%) and N (2.83 at%) species, which can provide some pseudocapacitance during

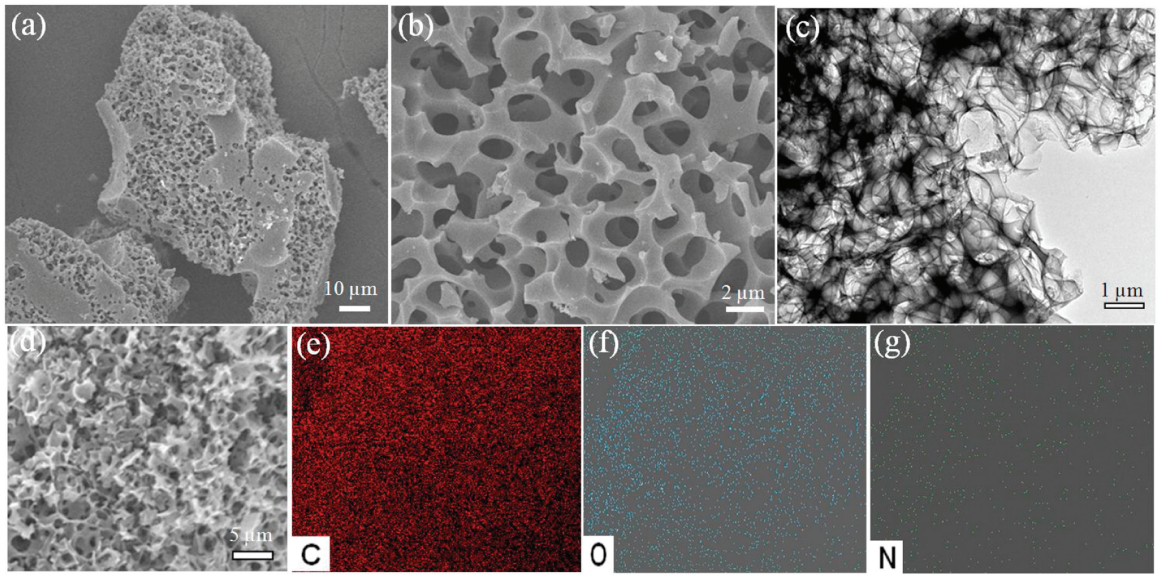

Fig. 1. (a, b) SEM images of NPC-700. (c) TEM image of NPC-700. (d) SEM image of NPC-700 and corresponding elemental mapping images of (e) C, (f) O and (g) N.

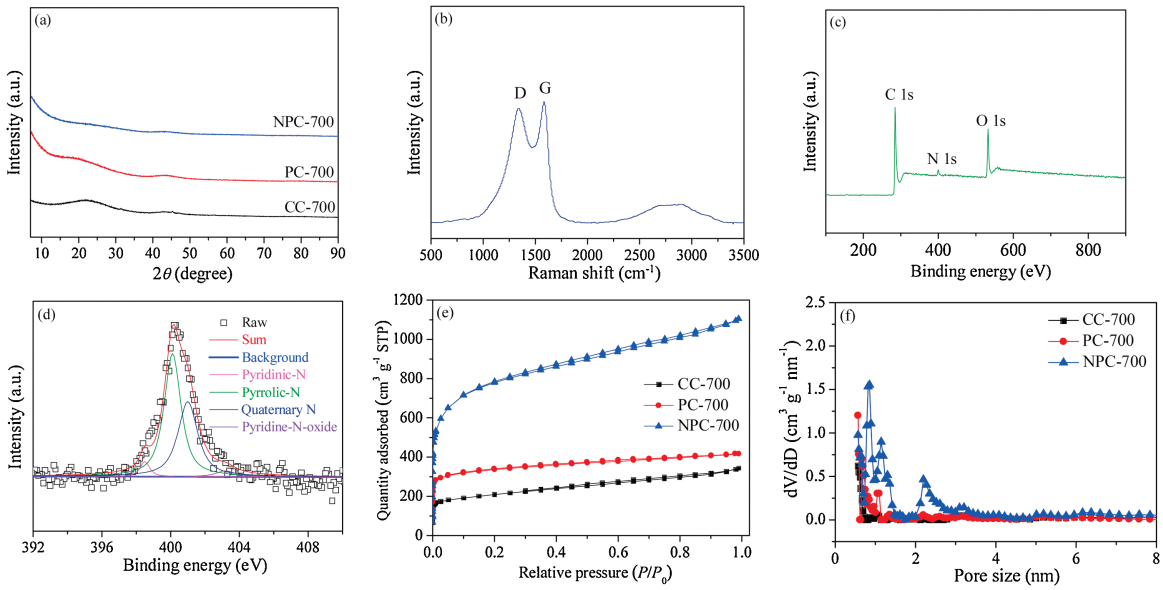

Fig. 2. (a) XRD curves of CC-700, PC-700 and NPC-700. (b) Raman spectrum of the NPC-700 sample. (c) XPS survey spectrum of NPC-700. (d) High-resolution XPS spectrum of N 1s for NPC-700 sample. (e) N_2 adsorption/desorption isotherms of CC-700, PC-700 and NPC-700. (f) Pore sizes distribution of the CC-700, PC-700 and NPC-700.

charge/discharge process. The high resolution N 1s spectrum of NPC-700 (Fig. 2d) can be divided into four peaks located at 398.5 eV, 400.2 eV, 401.1 eV and 403.2 eV, corresponding to pyridinic-N (3.78%), pyrrolic-N (54.23%), quaternary-N (38.99%) and pyridine-N-oxide (3%). High content of quaternary-N can greatly enhance the conductivity of carbon materials. The pore structure of all samples was further measured through nitrogen adsorption/desorption isotherms. The detailed pore structure information is listed in Table S1 (Supporting information). As seen in Fig. 2e, all materials display typical characteristic of I type adsorption-desorption isothermal and the adsorption curves increase sharply in the low-pressure range (P/P_0 <0.01), indicating massive micropores exist. The NPC-700 displays a high specific surface area of 2846 m^2/g, which is much higher than CC-700 (752 m^2/g) and PC-700 (1273 m^2/g) demonstrating that $KHCO_3$ and urea synergistic effect can greatly enhance the specific surface area. Moreover, the specific surface area increases from 1535 m^2/g (NPC-600) to 2846 m^2/g and finally slightly increase to 2848 m^2/g (NPC-800). The pore size distribution of NPC-700 (Fig. 2f) is mainly located at 0.6–1.8 nm and 2.0–3.5 nm, indicating hierarchical porous structure.

The electrochemical characteristics of the prepared samples were measured by cyclic voltammetry (CV) curve and galvanostatic charge-discharge (GCD) curve in 6 mol/L KOH. As presented in Fig. 3a, the CV curve of NPC-700 electrode displays larger integral area than CC-700 and PC-700, indicating that the NPC-700 electrode has the highest specific capacitance due to high surface area with massive heteroatoms functional groups. Moreover, the CV curve of NPC-700 electrode possesses slightly faradaic humps, indicating part contribution from pseudocapacitance. The possible surface redox reactions are as follows:

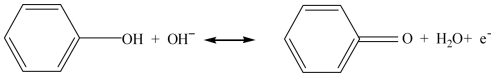

(1)

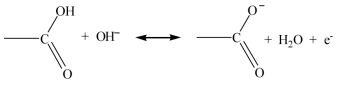

(2)

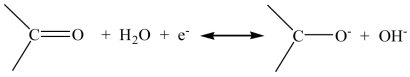

(3)

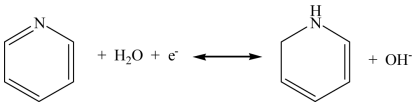

(4)

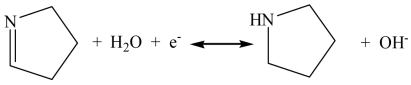

(5)

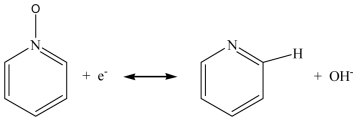

(6)

Even at 200 mV/s, the CV curves of NPC-700 electrode (Fig. 3b) can maintain rectangular-like shape without obvious distortion, demonstrating 3D hierarchical porous structure can ensure fast electron/ion transfer. Furthermore, with the increase of temperature, the redox peak of the NPC electrodes becomes weak due to high temperature is conducive to graphitization (Fig. S5a in Supporting information). Consistent with the CV results, the GCD profile of the NPC-700 electrode (Fig. 3c) also has the longest discharge time. The GCD curves of the NPC-700 electrode (Fig. 3d) show a symmetrical and nearly linear discharge character at various current densities, indicating perfect capacitive behavior. The specific capacitance of the NPC-700 electrode calculated by discharge curves is 324 F/g at 1 A/g (Fig. 3e), higher than those of CC-700 (190 F/g) and PC-700 (266 F/g). As presented in Fig. S5c (Supporting information), the NPC-700 electrode shows higher specific capacitance compared to NPC-600 (283 F/g) and NPC-800 (286 F/g) due to suitable specific surface area and heteroatom functional groups.

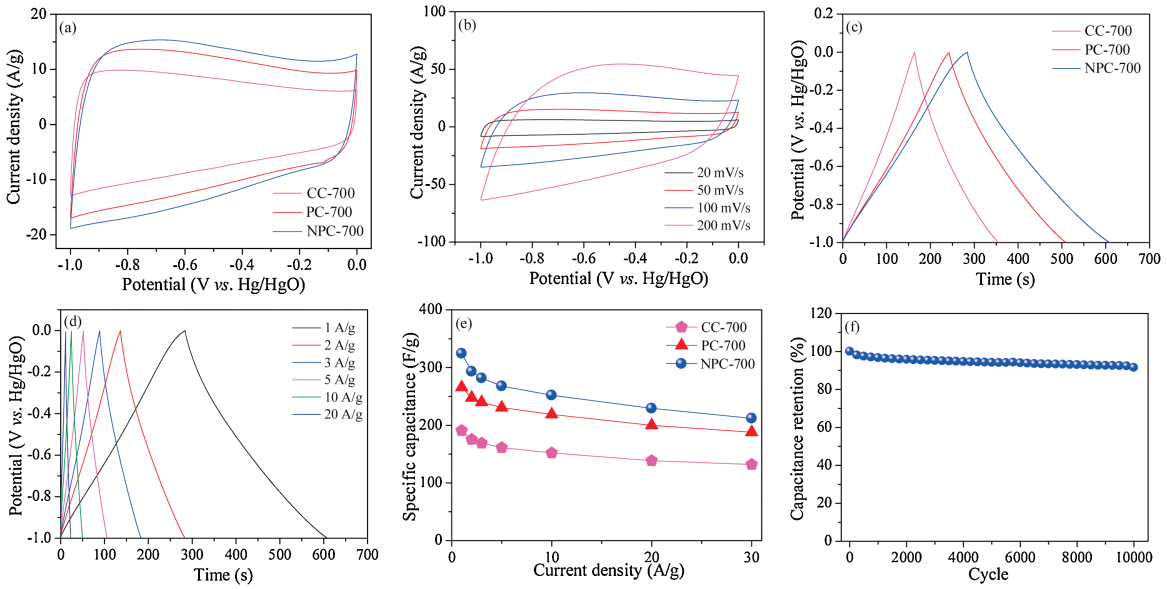

Fig. 3. (a) CV curves of CC-700, PC-700 and NPC-700 at 50 mV/s. (b) CV curves at different scan rates of NPC-700. (c) GCD curves of CC-700, PC-700 and NPC-700 at 1 A/g. (d) Charge-discharge curves of NPC-700 at different current density. (e) Specific capacitance of CC-700, PC-700 and NPC-700 at different current densities. (f) Cycling stability of NPC-700 after 10000 cycles.

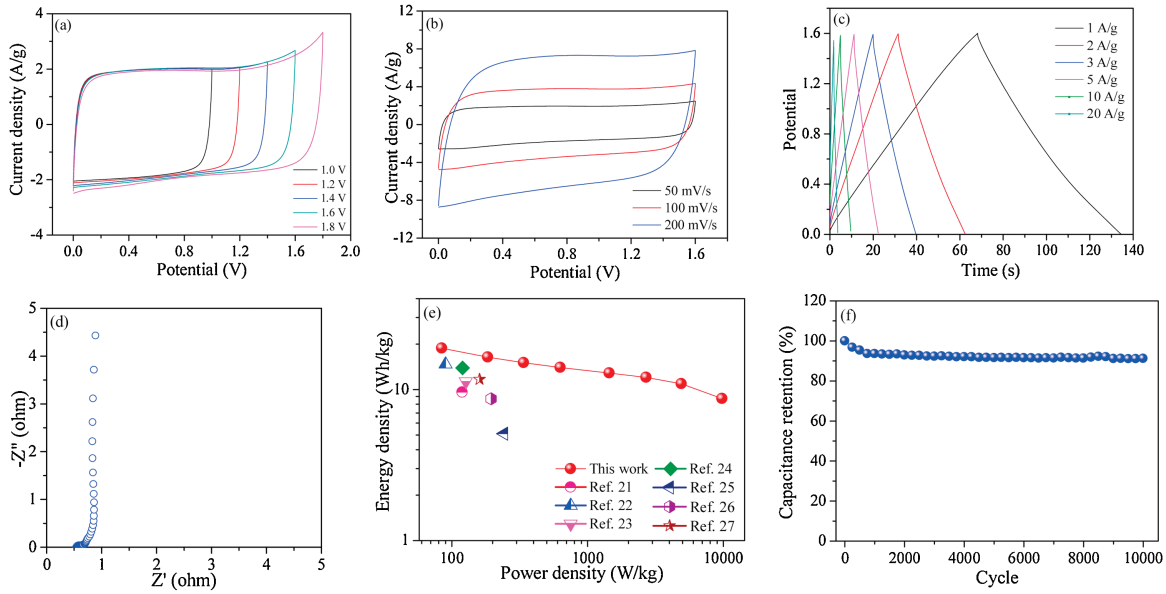

Fig. 4. (a) CV curves of the NPC-700//NPC-700 SC in different operation voltages at 50 mV/s. (b) CV curves of the NPC-700//NPC-700 SC at different scan rate from 50 mV/s to 200 mV/s. (c) GCD curves of the NPC-700//NPC-700 SC at different current density. (d) Nyquist plots of the NPC-700//NPC-700 SC. (e) Ragone plots of the NPC-700//NPC-700 SC and other previously reported carbon-based symmetric supercapacitors. (f) Electrochemical stability of the NPC-700//NPC-700 SC tested at 200 mV/s for 10000 cycles.

Furthermore, the specific capacitance of NPC-700 electrode (Fig. 3e) can maintain 212 F/g at 30 A/g with the capacitance retention of 65.4%, indicating superior rate characteristic. Moreover, the NPC-700 electrode can keep 91.5% capacitance retention rate after 10000 cycles (Fig. 3f), indicating good electrochemical stabilization.

To further characterize the outstanding electrochemical characteristic of the NPC-700, a symmetrical supercapacitor (SC) using the NPC-700 as both positive and negative electrodes was constructed and tested in 1 mol/L Na_2SO_4 electrolyte. Fig. 4a displays the CV profiles of the assembled SC at 50 mV/s in various voltage ranges. The curve displays nearly rectangular-like shapes in the voltage range of 0–1.6 V, demonstrating that such SC could be stable reversibly cycled in this voltage range. Even at 200 mV/s, the CV curves of SC (Fig. 4b) can keep rectangular-like shape without obvious distortion, demonstrating fast electron/ion transfer and good rate characteristic. The GCD profiles of the SC at various current densities are presented in Fig. 4c, all curves show highly linear and almost triangular shape, confirming excellent electrochemical reversibility. Fig. 4d displays the Nyquist plot of the NPC-700//NPC-700 SC, the ohmic resistance of the electrolyte and cell components is 0.55 Ω, suggesting excellent conductivity. Moreover, the NPC-700//NPC-700 SC shows an almost vertical line at a low-frequency scope, meaning rapid electron transfer. As shown in Fig. 4e, the energy density of the assembled SC can achieve 18.8 Wh/kg, which is much higher than that of other previously reported carbon-based materials [21–27]. In addition, the capacitance retention rate of the SC can achieve 91.3% after 10000 cycles (Fig. 4f), confirming excellent electrochemical stability.

In summary, we have demonstrated a facile method to synthesize O,N-codoped hierarchical porous carbon with ultra-high specific surface area and rich heteroatoms functional groups. Such porous carbon displays high specific capacitance, outstanding rate performance and good electrochemical stabilization. Moreover, the assembled symmetrical supercapacitor can achieve a high energy density of 18.8 Wh/kg and good electrochemical stabilization. These exciting results indicate that such porous carbon is a promising electrode material for supercapacitors.

Declaration of competing interest

The authors declared that they have no conflicts of interest to this work.

Acknowledgments

All authors are very grateful for the financial support of the National Natural Science Foundation of China (Nos. 51702043, 51672055 and 51972342), Heilongjiang Postdoctoral Foundation (No. LBH-Z18008).

Appendix A. Supplementary data

Supplementary material related to this article can be found, in the online version, at doi:https://doi.org/10.1016/j.cclet.2019.11.023.

References

[1] Q. Wang, J. Yan, Z. Fan, Energy Environ. Sci. 9 (2016) 729–762.
[2] D.W. Xiao, Q.Y. Dou, L. Zhang, et al., Adv. Funct. Mater. (2019) 1904136.
[3] M. Yang, Z. Zhou, Adv. Sci. 4 (2017) 1600408.
[4] L. Peng, Y. Liang, J. Huang, et al., ACS Sustain. Chem. Eng. 7 (2019) 10393–10402.
[5] S. Yang, S. Wang, X. Liu, L. Li, Carbon 147 (2019) 540–549.
[6] L. Qie, W. Chen, H. Xu, et al., Energy Environ. Sci. 6 (2013) 2497–2504.
[7] X. Wu, B. Ding, C. Zhang, et al., Carbon 153 (2019) 225–233.
[8] T. Liu, F. Zhang, Y. Song, Y. Li, J. Mater. Chem. A 5 (2017) 17705–17733.
[9] D. Guo, L. Zhang, X. Song, et al., New J. Chem. 42 (2018) 8478–8484.
[10] N. Sun, Z. Li, X. Zhang, et al., ACS Sustain. Chem. Eng. 7 (2019) 8735–8743.
[11] X. Hu, Y. Wang, B. Ding, et al., J. Alloys. Compd. 785 (2019) 110–116.
[12] G. Zhao, C. Chen, D. Yu, et al., Nano Energy 47 (2018) 547–555.
[13] W. Zhou, S. Lei, S. Sun, et al., J. Power Sources 402 (2018) 203–212.
[14] B. Ding, D. Guo, Y. Wang, et al., J. Power Sources 398 (2018) 113–119.
[15] Y. Li, Y. Liang, H. Hu, et al., Carbon 152 (2019) 120–127.
[16] C. Long, J. Zhuang, Y. Xiao, et al., J. Power Sources 310 (2016) 145–153.
[17] B. Liu, Y. Liu, H. Chen, et al., J. Power Sources 314 (2017) 309–317.
[18] Y. Wang, B. Ding, D. Guo, et al., Microporous Mesoporous Mater. 282 (2019) 114–120.
[19] C. Chang, H. Wang, Y. Zhang, et al., ACS Sustain. Chem. Eng. 7 (2019) 10763–10772.
[20] W. Yang, W. Yang, L. Kong, et al., Carbon 127 (2018) 557–567.
[21] Q. Wang, J. Yan, T. Wei, et al., Carbon 60 (2013) 481–487.
[22] H. Peng, G. Ma, K. Sun, et al., Electrochim. Acta 190 (2016) 862–871.
[23] Q. Wang, J. Yan, Y. Wang, et al., Carbon 52 (2013) 209–218.
[24] Y. Cheng, B. Li, Y. Huang, et al., Appl. Surf. Sci. 439 (2018) 712–723.
[25] Z. Liu, D. Fu, F. Liu, et al., Carbon 70 (2014) 295–307.
[26] S. Zuo, J. Chen, W. Liu, et al., Carbon 129 (2018) 199–206.
[27] Z. Wang, Y. Tan, Y. Yang, et al., J. Power Sources 378 (2018) 499–510.